

# Jitter and Amplitude Noise Accumulations in Cascaded All-Optical Regenerators

Zuqing Zhu, *Student Member, IEEE*, Masaki Funabashi, Zhong Pan, *Student Member, IEEE, Student Member, OSA*, Bo Xiang, Loukas Paraschis, and S. J. B. Yoo, *Senior Member, IEEE, Member, OSA*

**Abstract**—This paper proposes and demonstrates a simulation model to systematically investigate jitter accumulations in cascaded all-optical 2R regenerators. The simulation results indicate that when the pattern dependence from the memory effect is minimized, the jitter accumulation depends critically on the degree of the regenerative nonlinearity. Studies of tradeoffs between the jitter from bandwidth limitation and the signal-to-noise-ratio degradation help identify the optimized regenerator bandwidth for various degrees of regenerative nonlinearity. The simulation then considers the pattern dependence from the memory effect and finds that it can severely degrade the cascadability of an optical 2R regenerator and can make it worse than that of a linear optical amplifier (optical 1R). The simulation results show good matches to the experimental results of an optical 2R regenerator based on a semiconductor optical amplifier based Mach–Zehnder interferometer. To overcome the jitter accumulation associated with the optical 2R regeneration, we experimentally demonstrate an optical 3R regenerator for optical nonreturn-to-zero signals with all-optical clock recovery. The experiments achieve more than 1000-hop cascadability for pseudorandom binary sequence  $2^{31}-1$  inputs with a 100-km recirculation loop using lab fiber. Field trial experiments then demonstrate a more than 1000-hop cascadability for a 3R spacing of 66 km and a 100-hop cascadability for a 3R spacing of 264 km.

**Index Terms**—All-optical clock recovery, bit error rate (BER) simulation, clock enhancement, Fabry–Perot filter, jitter accumulation, optical regeneration, semiconductor optical amplifier (SOA)-based Mach–Zehnder interferometer (MZI).

## I. INTRODUCTION

THE deployment of all-optical regenerators in future optical networks may increase the transmission reach and allow for more flexible and efficient solutions compared to the O/E/O counterparts [1]–[4]. Optical regenerators using combinations of reamplification (1R), reshaping (2R), and retiming (3R) have been studied intensively. When evaluating these optical regenerators, the cascadability becomes an important issue [1], [5], [6]. Optical signal-to-noise (OSNR) degradations caused by optical amplifiers limit the cascadability of optical 1R regenerators [7]. Optical 2R regenerators utilize nonlinear transfer functions to

prevent amplitude noise from accumulation. When the retiming is absent, timing jitter accumulates and eventually imposes the necessity for full optical 3R regeneration [8].

Previous publications [5], [6] have theoretically investigated how the degree of nonlinearity affects the optical 2R cascadability when ignoring the timing jitter effects. However, experiments have found that jitter accumulation limits the cascadability of an optical 2R regenerator in a most interesting way [2], [9], [10]. Timing jitter usually consists of noise-induced random jitter and systematic jitter caused by bandwidth limitation, memory effect, and other system imperfections [11]–[13]. For all-optical 2R regenerators, experimental investigation indicated that systematic jitter dominates the jitter accumulation [2], [9], [10]. The situation becomes even worse when the systems employ the nonreturn-to-zero (NRZ) format, and memory-effect reduction technologies, such as differential operation [14] and spectrum slicing [8], are difficult to apply. Previous proposed theoretical models for simulating the jitter accumulation through cascaded optical 2R regenerators either only considered the noise-induced random jitter [3], [15] or depend on the assumption of linear jitter increment [9], [16]. As will be seen below, the systematic jitter increases nonlinearly when the regenerative nonlinearity is insufficient or the pattern dependence from the memory effect is severe. In this paper, we systematically investigate the jitter and amplitude noise accumulation in cascaded optical 2R regenerators with theoretical simulations and experimental measurements. The simulation model studies the individual and combinational effects from the degree of regenerative nonlinearity, bandwidth limitation, and pattern dependence and how they limit the optical 2R cascadability. The simulation results show a good match with the experimental results. To overcome the jitter accumulation associated with optical 2R regeneration, we then experimentally demonstrate an optical 3R regenerator for optical NRZ signals. Field trial experiments are also included to investigate the stability of the optical 3R regenerator in a relatively realistic condition and the tradeoff between the cascadability and regeneration spacing.

The rest of this paper is organized as follows. Section II presents the theoretical model of optical 2R regeneration to simulate the jitter and amplitude noise accumulation. Section III discusses the theoretical and experimental investigation on the cascadability of an optical 2R regenerator based on semiconductor optical amplifier (SOA)-based Mach–Zehnder interferometer (MZI). Section IV shows the experimental demonstration of an optical 3R regenerator for optical NRZ signals. Section V summarizes this paper.

Manuscript received June 28, 2007; revised October 30, 2007.

Z. Zhu, M. Funabashi, Z. Pan, B. Xiang, and S. J. B. Yoo are with the Department of Electrical and Computer Engineering, University of California, Davis, CA 95616 USA (e-mail: zqzhu@ece.ucdavis.edu; funa@ucdavis.edu; zhopan@ece.ucdavis.edu; boxiang@ucdavis.edu; yoo@ece.ucdavis.edu).

L. Paraschis is with the Optical Networking Advanced Technology Group, Cisco Systems, San Jose, CA 95134 USA (e-mail: loukas@cisco.com).

Color versions of one or more of the figures in this paper are available online at <http://ieeexplore.ieee.org>.

Digital Object Identifier 10.1109/JLT.2008.919484

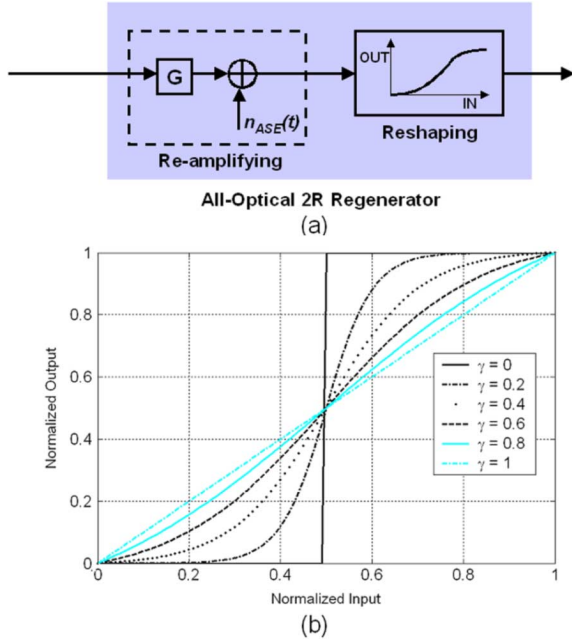


Fig. 1. (a) Simplified all-optical 2R regenerator model for noise analysis. (b) Normalized nonlinear transfer functions with different  $\gamma$  parameters.

## II. THEORETICAL MODEL OF OPTICAL 2R REGENERATOR

Optical 2R regeneration relies on the nonlinear transfer function to redistribute the amplitude noise added by optical amplifiers. Theoretical analysis [6] and experimental investigations [17] have proven that this noise-redistribution property can suppress the bit error rate (BER) accumulation due to amplitude noise in a cascade of fiber links. On the other hand, previous theoretical and experimental work also verified that the imperfections associated with realistic optical 2R regenerators, such as bandwidth limitation and pattern dependence induced by memory effect, can induce timing jitter and greatly limit the device cascadability [3], [13], [17], [18]. Here, memory effect means that the response of a current bit can be affected by the pattern of the preceding bits [3], [13], [17], [18]. In this section, we start from a simplified 2R regenerator model that only includes the nonlinear transfer function [6] and gradually includes bandwidth limitation and pattern-dependence effects. In Section II-D, we propose a theoretical model to simulate the amplitude- and jitter-noise accumulation in realistic optical 2R regenerators and to predict the device cascadability.

### A. Model of Amplitude Noise Suppression

Fig. 1(a) shows the diagram of a simplified optical 2R regenerator model [5], [6] that only considers the signal levels for noise analysis and ignores dynamic effects, memory effects, and jitter. The model decomposes an all-optical 2R regenerator into a linear amplifier and a nonlinear reshaping element. The reshaping element is represented by a nonlinear transfer function [5], [6]

$$\begin{cases} f(x) = a \cdot \tanh(b(x - 0.5)) + 0.5 \\ f(0) = 0 \\ f'(0.5) = 1/\gamma \end{cases} \quad (1)$$

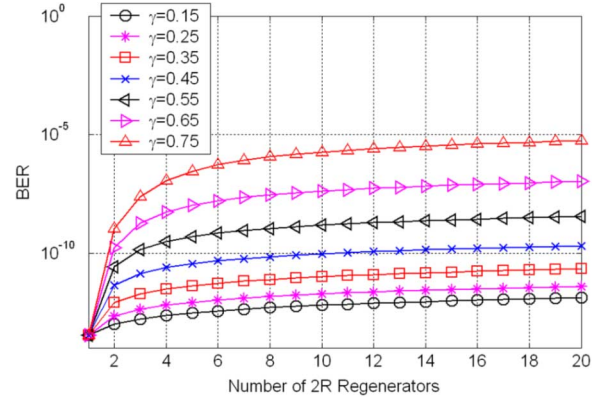


Fig. 2. BER evolution for 2R regenerator with different  $\gamma$  parameters.

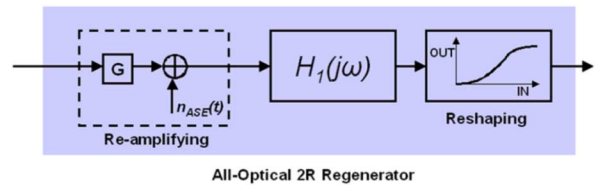


Fig. 3. Simulation model of all-optical 2R regenerator that considers the bandwidth limitation of the device.

Here,  $x$  represents the input signal level ranging from zero to one,  $a$  and  $b$  are constants that normalize  $f(x)$  within  $(0, 1)$ , and  $\gamma$  is the parameter to characterize the degree of the nonlinearity. The  $\gamma$  parameter changes  $f(x)$  from a step function (perfect nonlinear thresholding) when  $\gamma \rightarrow 0$  to a linear-slope-ramp function (no nonlinear thresholding) when  $\gamma = 1$  [6]. Fig. 1(b) plots the nonlinear transfer functions for various  $\gamma$  parameters. With this model and the noise analysis method proposed in [6], we simulate the BER accumulation through 2R regeneration stages for various  $\gamma$  parameters. We assume the initial BER is  $3.31 \times 10^{-14}$  after the first optical 2R regenerator (initial Q factor = 7.35). Fig. 2 plots the simulation results. The results indicate that the evolution of the BER induced by amplitude noise is critically dependent on the  $\gamma$  parameter.

### B. Bandwidth Limitation Effects

We then consider the frequency response of the all-optical 2R regenerator. Fig. 3 shows the diagram of the simulation model that includes the frequency response of the optical 2R. Here,  $H_1(j\omega)$  represents the transfer function of the device. To restrict the noise entering into the reshaping element,  $H_1(j\omega)$  should possess a low-pass filtering property [16]. In practical optical 2R regenerators, the device properties, such as carrier dynamics, can intrinsically limit the bandwidth [14], [19]. To isolate problems, we assume that  $H_1(j\omega)$  induces minimal pattern-dependent jitter. One practical realization of  $H_1(j\omega)$  for validating the assumption is the Bessel filter function [13]. In the following simulation,  $H_1(j\omega)$  takes the shape of a fifth-order Bessel filter with a 3-dB cutoff frequency of  $f_1 = \beta/T_0$ . Here,  $T_0$  is the one-bit duration of the input signal (e.g.,  $T_0$  equals 100 ps for 10 Gb/s simulation) and  $\beta$  is the bandwidth enhancement factor. The parameter  $T_0$  is fixed at 100 ps (10 Gb/s operation) for all

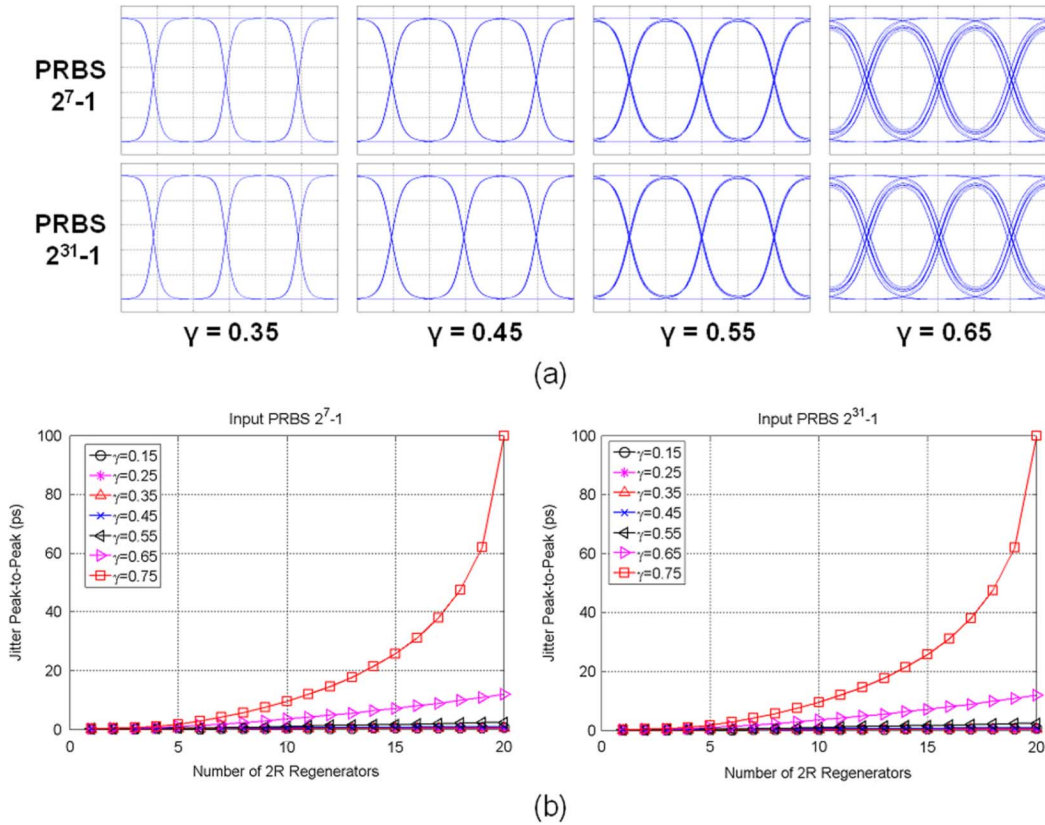


Fig. 4. (a) Simulated 10 Gb/s eye diagrams after 20 cascaded optical 2R regenerators with  $\beta = 1$ . (b) Jitter peak-to-peak evolution for PRBS lengths of  $2^7-1$  and  $2^{31}-1$ .

of the simulations in this paper, while similar results can be applied to other bit rates.

Fig. 4(a) shows the simulated 10 Gb/s eye diagrams of signals after 20 cascaded optical 2R regenerators with  $\beta = 1$  for input pseudorandom bit sequence (PRBS) lengths of  $2^7-1$  and  $2^{31}-1$ . The eye diagrams for signals with different PRBS lengths are almost identical when the  $\gamma$  parameter of the regenerator is the same. These results verify our assumption that  $H_1(j\omega)$  induces minimal pattern-dependent jitter. The jitter accumulation observed in Fig. 4(a) is from the waveform distortion caused by cascaded low-pass filtering operations. When the regenerator does not have enough reshaping nonlinearity to recover the waveform distortion, it can induce severe jitter accumulation. This jitter accumulation is solely from the bandwidth limitation of the device. Fig. 4(b) shows the jitter peak-to-peak evolution for PRBS lengths of  $2^7-1$  and  $2^{31}-1$ . The simulation shows that the jitter accumulation is nonlinear when the  $\gamma$  parameter is larger than 0.65. Several previous proposed jitter models relied on the assumption that the jitter accumulation is linear through cascaded optical 2R regenerators [9], [16]. The results in Fig. 4(b) indicate that the linear jitter accumulation

assumption is only applicable when the 2R regenerators have sufficient nonlinearity (i.e.,  $\gamma < 0.65$ ). The simulation shows that the jitter accumulation is also critically dependent on the  $\gamma$  parameter when the pattern dependence is minimized.

The BER simulation uses an ideal integrate-and-dump receiver to recover the bit stream. The receiver sampling clock is assumed to be free of jitter. We ignored the clock imperfection from the receiver synchronization mechanism. More sophisticated and complicated receiver models that consider receiver-timing imperfection from clock recovery and sampling are available in [13]. Note that due to the jitter discussed above, the signal integral over one-bit duration is not identical for all "1" bits any more. As  $H_1(j\omega)$  achieves minimal pattern-dependent jitter, we can consider the closest bit-neighbors only [16]. For a "1" bit, there are four sequences with equal possibility: 010, 011, 110, and 111. Simulation obtains the integral of the "1" symbol in these sequences after cascaded 2R operations. Defining the integral results as  $E_{n,010}$ ,  $E_{n,011}$ ,  $E_{n,110}$ , and  $E_{n,111}$  for the "1" symbol in different sequences after  $n$  all-optical 2R regenerators, the BER can be written as shown in (2) at the bottom of the page. Here,  $D$  is the decision threshold

$$\begin{cases} \text{BER}_1 = \frac{1}{4} \left[ Q \left( \frac{E_{1,010} - D}{\sigma_1} \right) + Q \left( \frac{E_{1,011} - D}{\sigma_1} \right) + Q \left( \frac{E_{1,110} - D}{\sigma_1} \right) + Q \left( \frac{E_{1,111} - D}{\sigma_1} \right) \right] \\ \text{BER}_n = \frac{1}{4} \left[ Q \left( \frac{E_{n,010} - D}{\sigma_n} \right) + Q \left( \frac{E_{n,011} - D}{\sigma_n} \right) + Q \left( \frac{E_{n,110} - D}{\sigma_n} \right) + Q \left( \frac{E_{n,111} - D}{\sigma_n} \right) \right] + \text{BER}_{n-1} \end{cases} \quad (2)$$

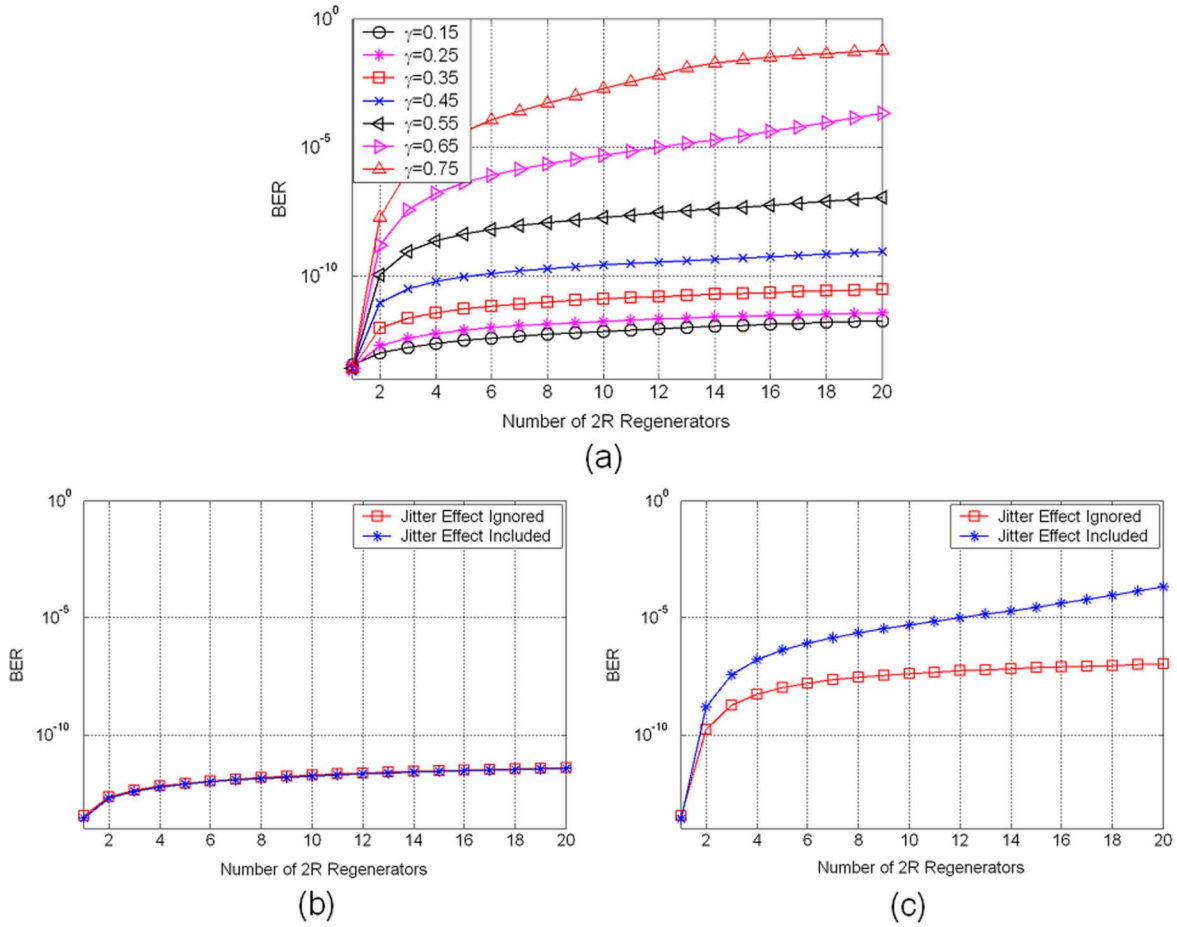


Fig. 5. BER simulation results for  $\beta = 1$  and input PRBS length of  $2^{31}-1$ . (a) BER evolution when including the jitter effect from bandwidth limitation, (b) BER comparison for  $\gamma = 0.25$ , and (c) BER comparison for  $\gamma = 0.65$ .

and  $Q(x) = (1)/(2)\text{erfc}(x)/(\sqrt{2})$  is the Q function [16]. For simplicity, a fixed  $D = E_0/2$  is used in the simulation and  $E_0 = \int_0^{T_0} g(t)dt$  is the integral of an initial “1” symbol. In the 2R regeneration operation, the amplifier noise term is approximated using a linear transformation with slope  $\gamma$  [6]

$$\begin{cases} \sigma_1^2 = \sigma_{\text{ASE}}^2 \\ \sigma_n^2 = \gamma^2 \sigma_{n-1}^2 + \sigma_{\text{ASE}}^2 \end{cases} \quad (3)$$

where  $n$  represents the number of cascaded all-optical 2R regenerators and  $\sigma_{\text{ASE}}^2$  is the variance of the amplifier noise. Previous work in [6] has proven that this approximation is an appropriate representation for modeling the dominant noise component in optical regenerators when the reamplification gain is reasonably large ( $>10$  dB) as in typical cases [6], [20].

Fig. 5 shows the BER simulation results for  $\beta = 1$  and input PRBS length of  $2^{31}-1$ . Fig. 5(a) plots the BER evolution when the jitter effect from bandwidth limitation is included. Fig. 5(b) and (c) compares the BER curves in Fig. 5(a) to the simulation results ignoring the jitter effect (as in Fig. 2). The BER comparisons indicate that when the  $\gamma$  parameter is relatively small (e.g., 0.15 or 0.25), errors from amplifier noise dominate the BER and the jitter effect can be ignored without affecting the simulation accuracy. However, when the  $\gamma$  parameter is larger than 0.65,

errors from the jitter effect will dominate the BER and it cannot be ignored anymore.

The above simulations prove that bandwidth limitation induces jitter and limits the cascadability of all-optical 2R regenerators. However, any increase in bandwidth corresponds to a decrease in the signal-to-noise ratio (SNR). If we assume the noise spectral density is constant and  $\sigma_{\text{ASE}}^2$  is the noise variance when bandwidth enhancement factor  $\beta = 1$ , then the noise variance for a 2R regenerator with an arbitrary bandwidth is

$$\sigma_{\text{ASE},\beta}^2 = \beta \cdot \sigma_{\text{ASE}}^2. \quad (4)$$

Substituting  $\sigma_{\text{ASE}}^2$  in (2) with  $\sigma_{\text{ASE},\beta}^2$ , we can simulate the tradeoff between bandwidth limitation and SNR degradation. Fig. 6 plots the effects of bandwidth enhancement factor  $\beta$  on BER evolution. Reducing the regenerator bandwidth limits the amplifier noise entering into the reshaping element and thus decreases the initial BER and the BER increment due to amplitude noise in each hop. On the other hand, the small regenerator bandwidth contributes to the jitter accumulation. Fig. 7 shows the BER after 20 cascaded optical 2R regenerators for the combinations of  $\gamma$  and  $\beta$ . In terms of the BER after 20 cascaded 2R regenerators, the optimal value of  $\beta$  is less than one when  $\gamma < 0.55$ , while optimal  $\beta$  is larger than one when  $\gamma$  equals 0.65 and 0.75. This is consistent with the results in Fig. 5. For small  $\gamma$  parameters, errors from the amplitude noise dominate

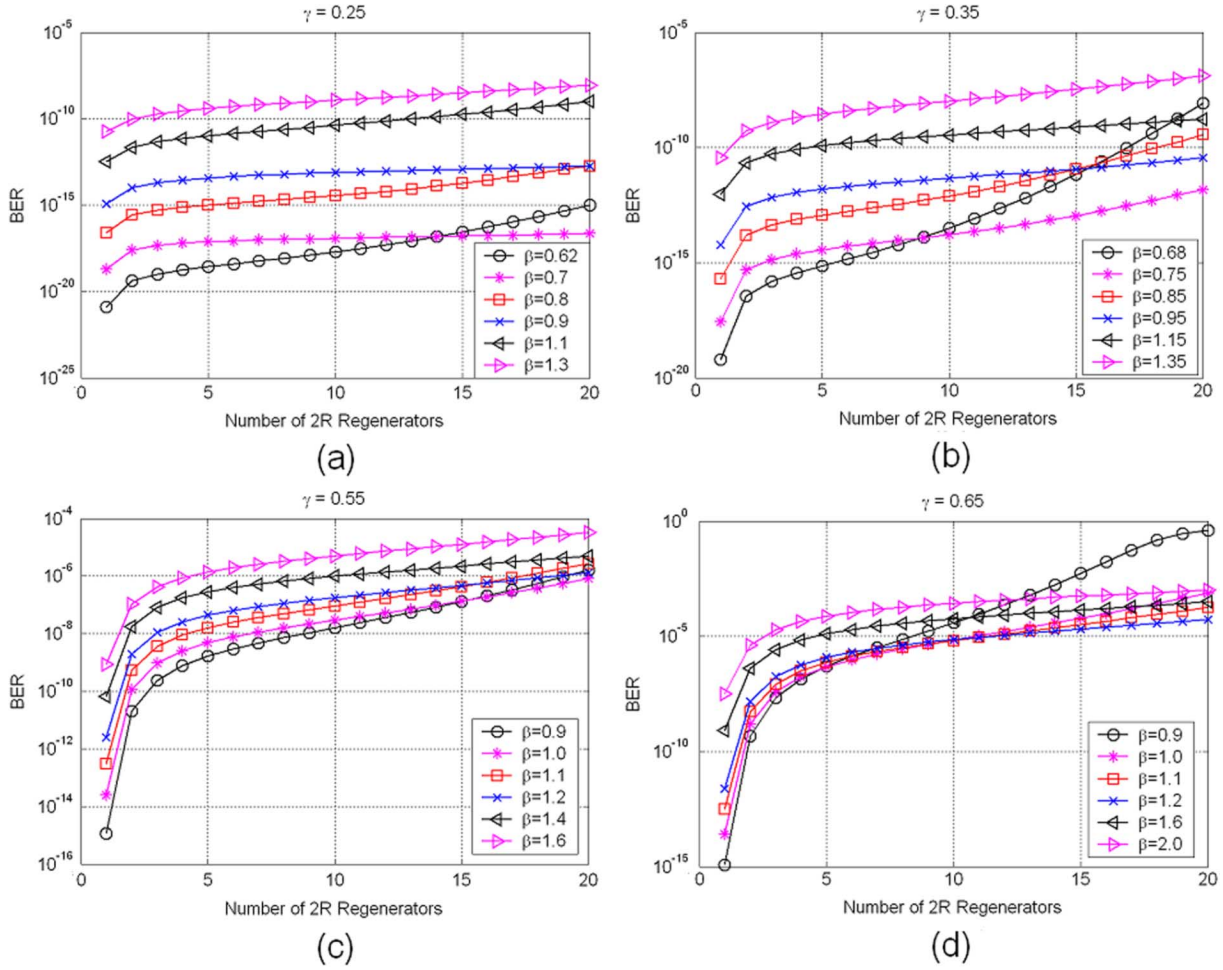


Fig. 6. Effects of bandwidth enhancement factor  $\beta$  on BER evolution.  $\gamma$  parameter of optical 2R regenerators are (a) 0.25, (b) 0.35, (c) 0.55, and (d) 0.65.

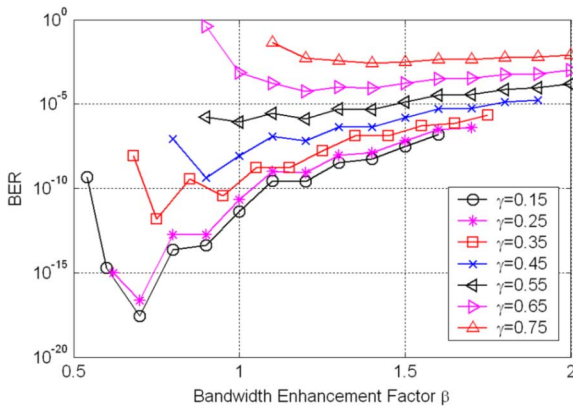


Fig. 7. BER after 20 optical 2R regenerators for the combinations of  $\gamma$  and  $\beta$ .

the BER. Reducing the bandwidth can effectively restrict the amplifier noise, and the extra jitter-tolerance margin from the regenerator nonlinearity can overcome the jitter accumulation from the bandwidth limitation. A large  $\gamma$  parameter makes the jitter-tolerance margin insufficient, and we need to sacrifice the SNR to relieve the jitter accumulation.

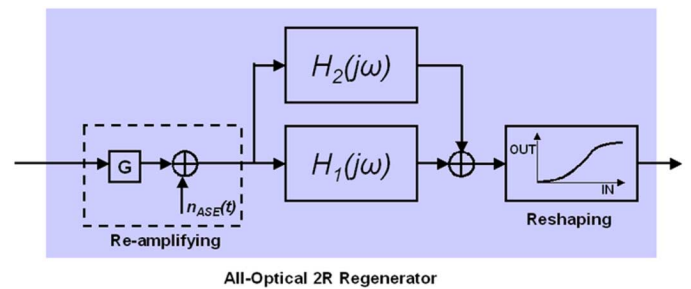


Fig. 8. Block diagram of an all-optical 2R regenerator model that includes pattern-dependence effect.

C. Pattern-Dependence Effects

Pattern dependence arises from the limited speed of the regeneration devices [12], [13], such as the finite gain recovery time of SOA devices [14], [19]. One simplified model of the memory effect is to emulate it with a linear filter  $H_2(j\omega)$  [9], [21]. We define the impulse response  $h_2(t)$  of  $H_2(j\omega)$  as [9]

$$h_2(t) = \begin{cases} a \cdot e^{-t/bT_0}, & t \geq 0 \\ 0, & t < 0 \end{cases} \quad (5)$$

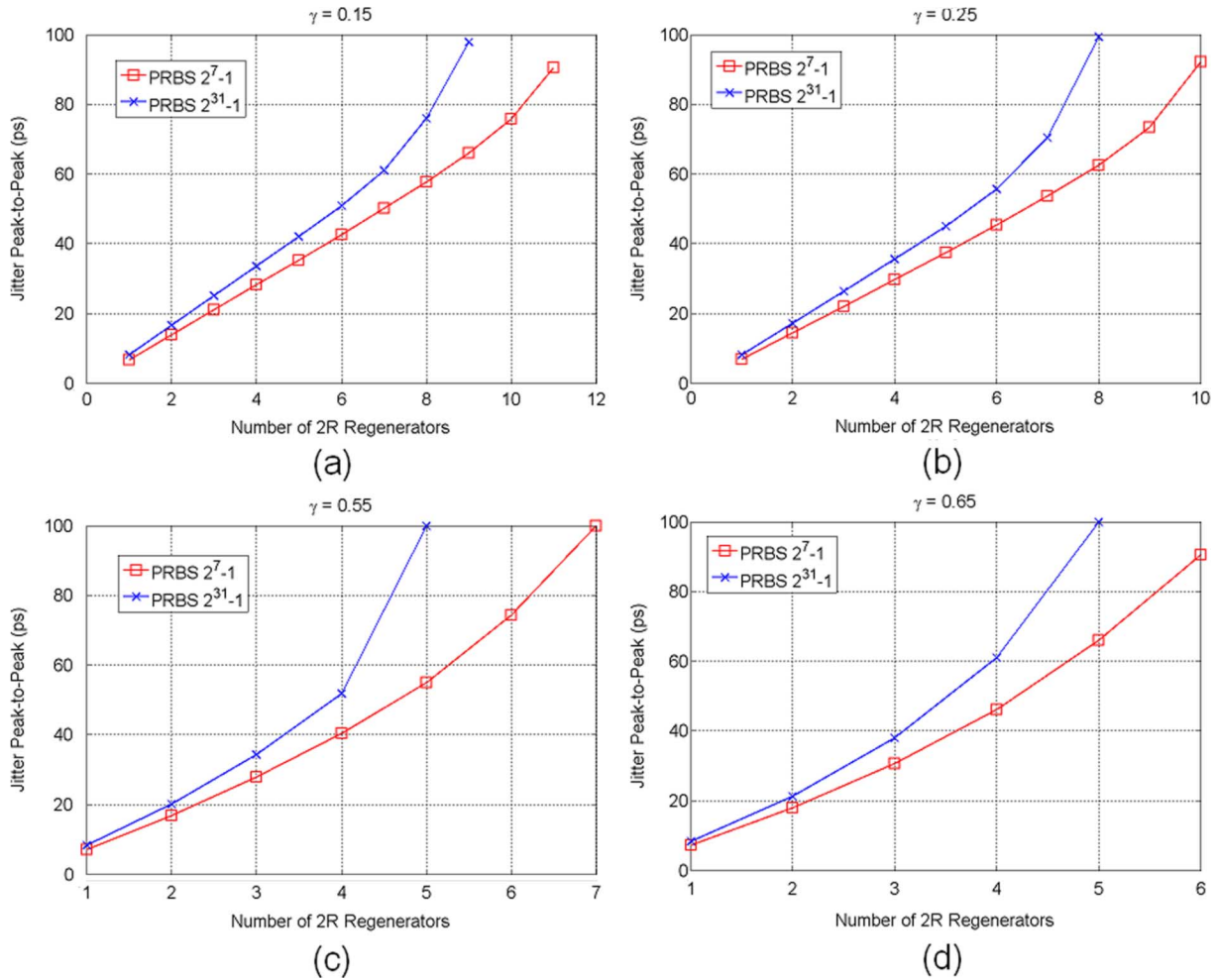


Fig. 9. Jitter accumulations when  $\gamma$  parameter is (a) 0.15, (b) 0.25, (c) 0.55, and (d) 0.65.

Here,  $a$  and  $b$  are the coefficients to quantify the pattern dependence and can be obtained by fitting measurement data to simulation results. This model ignores the wavelength dependence and chirp effect of the 2R regenerator devices. For optical 2R regenerators based on SOA-based interferometers, the wavelength dependence is relatively small, and a 0.5 dB receiver-penalty variation has been reported in [19] for 5 Gb/s wavelength conversion over a 30 nm range. The interferometric SOA regenerator can also optimize the chirp effect by biasing the input signal properly [19], [22]. Fig. 8 shows the modified simulation model to include the pattern-dependence effect. The parameters are  $a = 0.2$ ,  $b = 5$ , and  $\beta = 1$  in the simulation. Fig. 9 shows the jitter accumulations through 2R regeneration stages with various  $\gamma$  parameters. As expected, the jitter accumulation is much worse than that in Fig. 4(b) due to the pattern dependence. Longer PRBS sequence length induces larger jitter accumulation. This trend can be observed more clearly with the

eye-diagram comparisons in Fig. 10 when the  $\gamma$  parameter is fixed at 0.55.

Since the pattern dependence is included, BER simulation has to consider all possible bit-patterns and then averages the error rate over the possibility of the bit pattern to obtain the total BER. This method is not practical when the PRBS sequence length is long (e.g., PRBS  $2^{31}-1$ ). In order to complete the simulation with limited computational resources, we have to refine the bit patterns used in the BER simulation. It has been proven [9], [12] that the “1” bit that is most prone to errors is a single “1” bit preceded by a sequence of consecutive “0” bits. Since the longest length of consecutive zeroes is  $M-1$  in a  $2^M-1$  PRBS sequence, we can only consider these  $M-1$  sequences to estimate the total BER. We define that the possibility of  $m$  consecutive “0” bits is  $P_M(m)$  in a  $2^M-1$  PRBS sequence, and the integral result of the following single “1” symbol is  $E_m(n, \gamma)$ . Here,  $n$  represents the number of 2R regenerators the signal ex-

$$\begin{cases} \text{BER}_1 = \frac{1}{4} \sum_{m=1}^{M-1} P_M(m) \cdot Q\left(\frac{E_m(1, \gamma) - D}{\sigma_1}\right) + \frac{3}{4} Q\left(\frac{E_0}{2\sigma_1}\right) \\ \text{BER}_n = \frac{1}{4} \sum_{m=1}^{M-1} P_M(m) \cdot Q\left(\frac{E_m(n, \gamma) - D}{\sigma_n}\right) + \frac{3}{4} Q\left(\frac{E_0}{2\sigma_n}\right) + \text{BER}_{n-1} \end{cases} \quad (6)$$

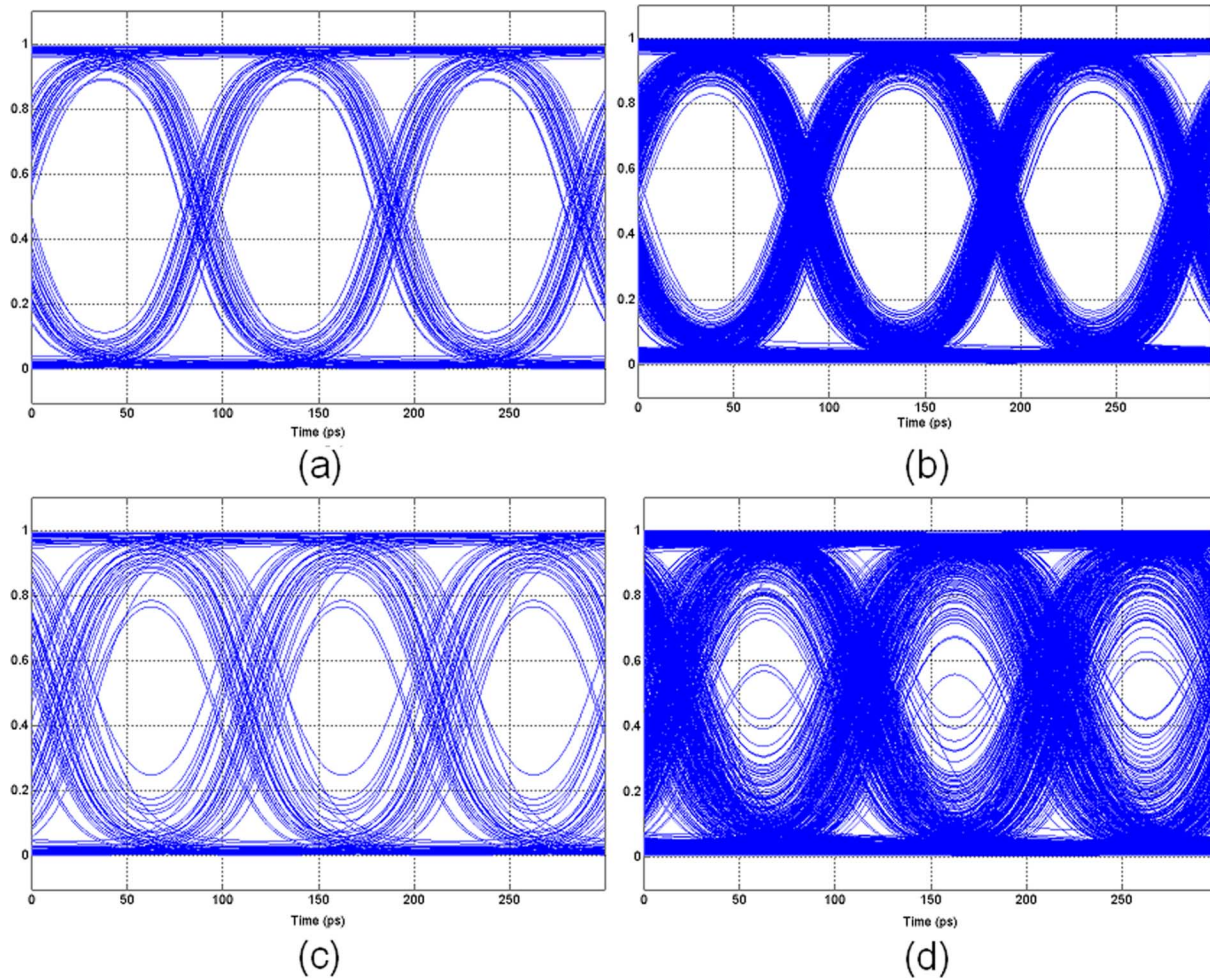


Fig. 10. Eye diagrams after three cascaded optical 2R regenerators for (a) PRBS  $2^7-1$  and (b) PRBS  $2^{31}-1$  and after five regenerators for (c) PRBS  $2^7-1$  and (d) PRBS  $2^{31}-1$ .

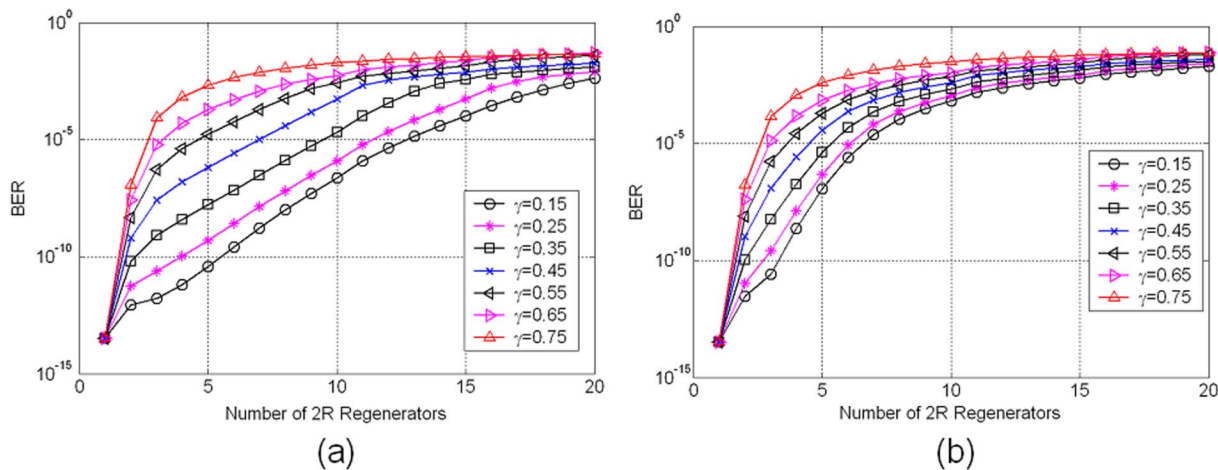


Fig. 11. BER evolution for (a) PRBS  $2^7-1$  and (b) PRBS  $2^{31}-1$  with  $a = 0.2, b = 5$ , and  $\beta = 1$ .

perceived. Then, the total BER can be approximated as shown in (6) at the bottom of the previous page. Here,  $\sigma_n, D$ , and  $E_0$  are the same as defined in Section II-B. Fig. 11 shows the BER simulation results for PRBS  $2^7-1$  and PRBS  $2^{31}-1$  with  $a = 0.2, b = 5$ , and  $\beta = 1$ . Fig. 12 shows the BER evolution comparisons between PRBS  $2^7-1$  and PRBS  $2^{31}-1$ .

#### D. Optical 2R Cascadability

When the optical reshaping device is absent, the optical regenerator becomes a “1R” regenerator only including an optical amplifier. In this section, we compare the cascadability of optical 1R and 2R regenerators with simulations. In most cases, the

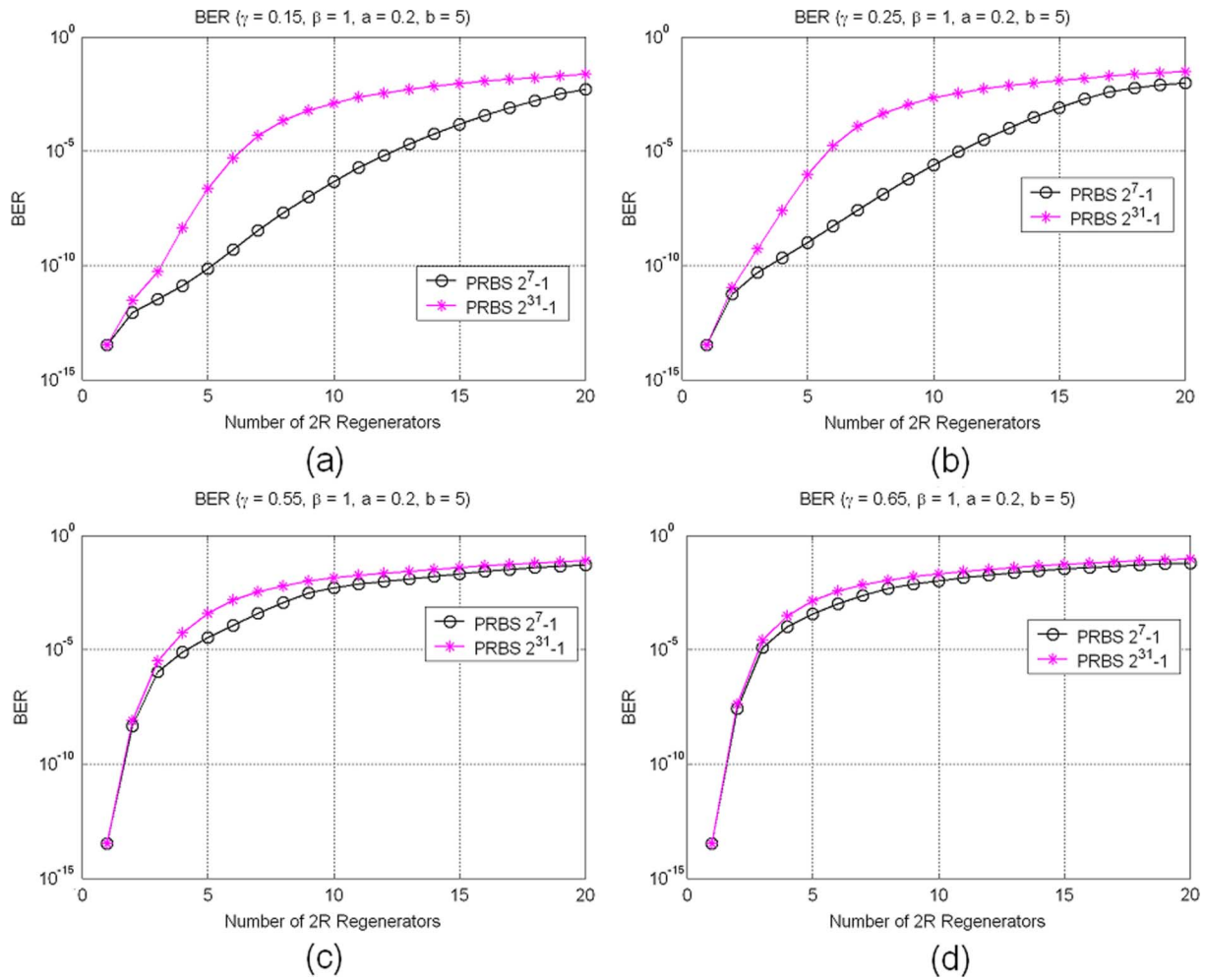


Fig. 12. BER evolution comparisons when  $\beta = 1$ ,  $a = 0.2$ ,  $b = 5$ , and  $\gamma$  is (a) 0.15, (b) 0.25, (c) 0.55, and (d) 0.65.

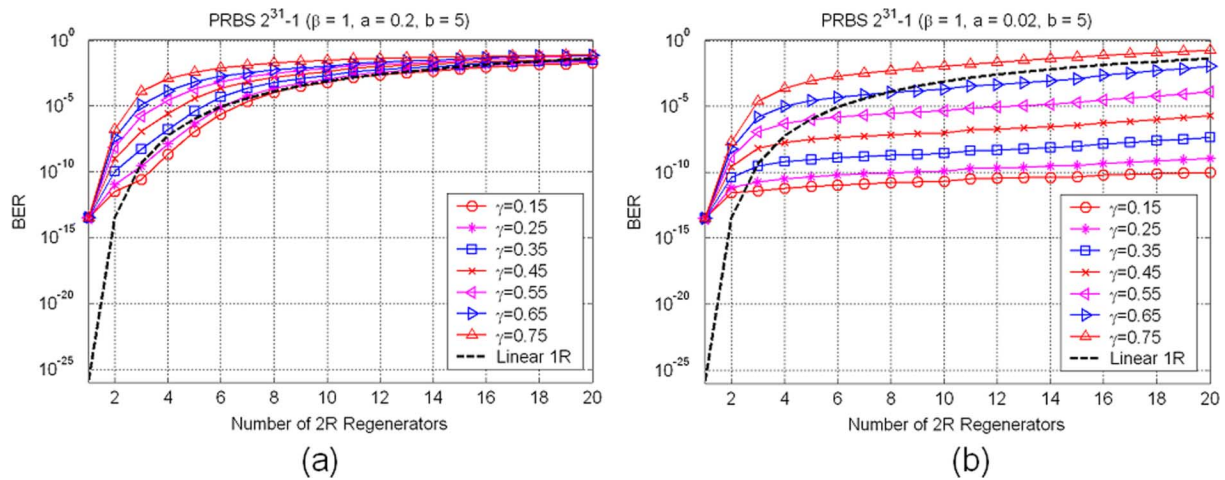


Fig. 13. Cascadability comparison for optical 1R and 2R:(a)  $\beta = 1$ ,  $a = 0.2$ ,  $b = 5$  and (b)  $\beta = 1$ ,  $a = 0.02$ ,  $b = 5$ .

optical reshaping device is also an active device associated with noise addition [1]. Thus, we cannot simply remove the filters and the reshaping element in Fig. 8 to model an optical 1R regenerator. Considering the noise contribution from the optical

amplifier and the optical reshaping device, the variance of the noise can be written as

$$\sigma_{\text{ASE}}^2 = \sigma_{\text{reamplifying}}^2 + \sigma_{\text{reshaping}}^2. \quad (7)$$

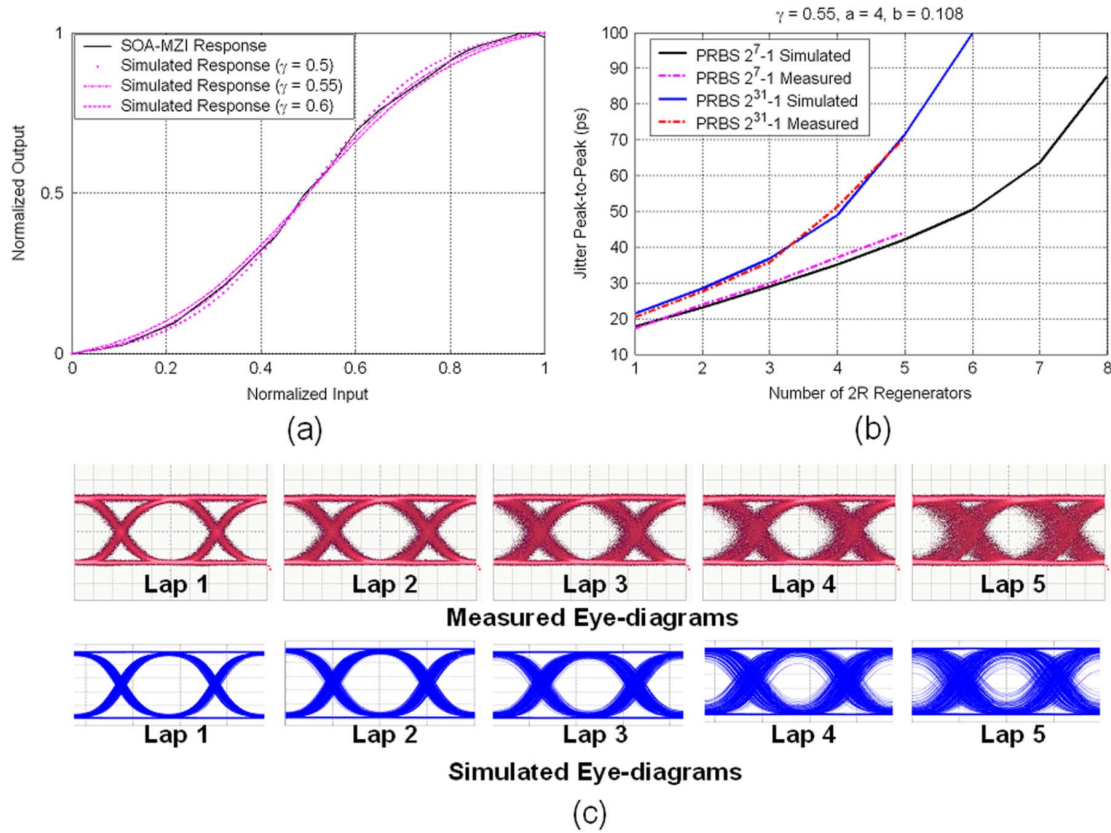


Fig. 14. (a) Curve fitting of the measured optical 2R transfer function after normalization, (b) measured and simulated jitter accumulation, and (c) measured and simulated eye-diagrams for PRBS  $2^{31}-1$ .

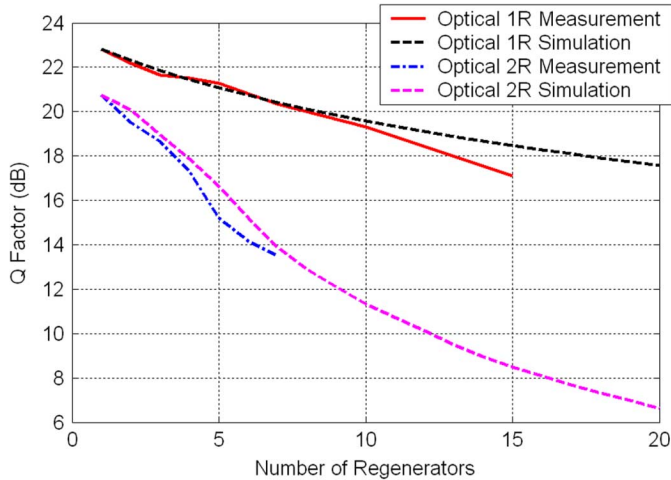


Fig. 15. Q factor evolution from simulation and measurement for optical 1R and 2R regeneration.

We assume  $\sigma_{\text{reamplifying}}^2 = \sigma_{\text{reshaping}}^2$  for the simulations in the rest of this section. Fig. 13 shows the cascability comparisons for optical 1R and 2R. When the pattern dependence is large ( $a = 0.2$ ), the optical 2R regenerator has to have an almost ideal nonlinear transfer function ( $\gamma \leq 0.15$ ) to outperform the optical 1R. With lower pattern dependence ( $a = 0.02$ ), the optical 2R regenerator can outperform optical 1R with a  $\gamma$  parameter of 0.65. These results indicate that the pattern dependence in the

optical 2R regenerator can severely decrease its cascability and that optical 2R regeneration can be worse than optical 1R regeneration (linear amplification).

### III. OPTICAL 2R REGENERATION USING SOA-MZI

The monolithic integrated [23] SOA-MZI is a compact building block for optical 2R regeneration. We investigate the regeneration performance of an SOA-MZI based optical 2R regenerator with experimental measurements and simulations in this section. The optical 2R regenerator consists of two cascaded SOA-MZIs.

Fig. 14(a) shows the curve-fitting results of the measured transfer function after normalization, and a  $\gamma$  parameter of 0.55 is obtained. In the experiments, the NRZ signal from the optical transmitter is not free of jitter. We introduce random jitter onto the initial signal to make the jitter simulation more accurate. We then obtain  $a = 4, b = 0.108$ , and  $\beta = 1.0$  by fitting the jitter measurement results to the simulation results. Fig. 14(b) shows the comparison of the measured and simulated jitter accumulations on a 10 Gb/s optical NRZ signal. Fig. 14(c) shows the measured and simulated eye diagrams for PRBS  $2^{31}-1$  input. It can be seen that the proposed simulation model can present the optical 2R regenerator with a reasonably good approximation. Fig. 15 shows the Q factor evolution from simulation and measurement for optical 1R and 2R regenerators. The input signals have a PRBS length of  $2^{31}-1$  at 10 Gb/s. The optical 2R regenerator is modeled with the parameters obtained above. Both

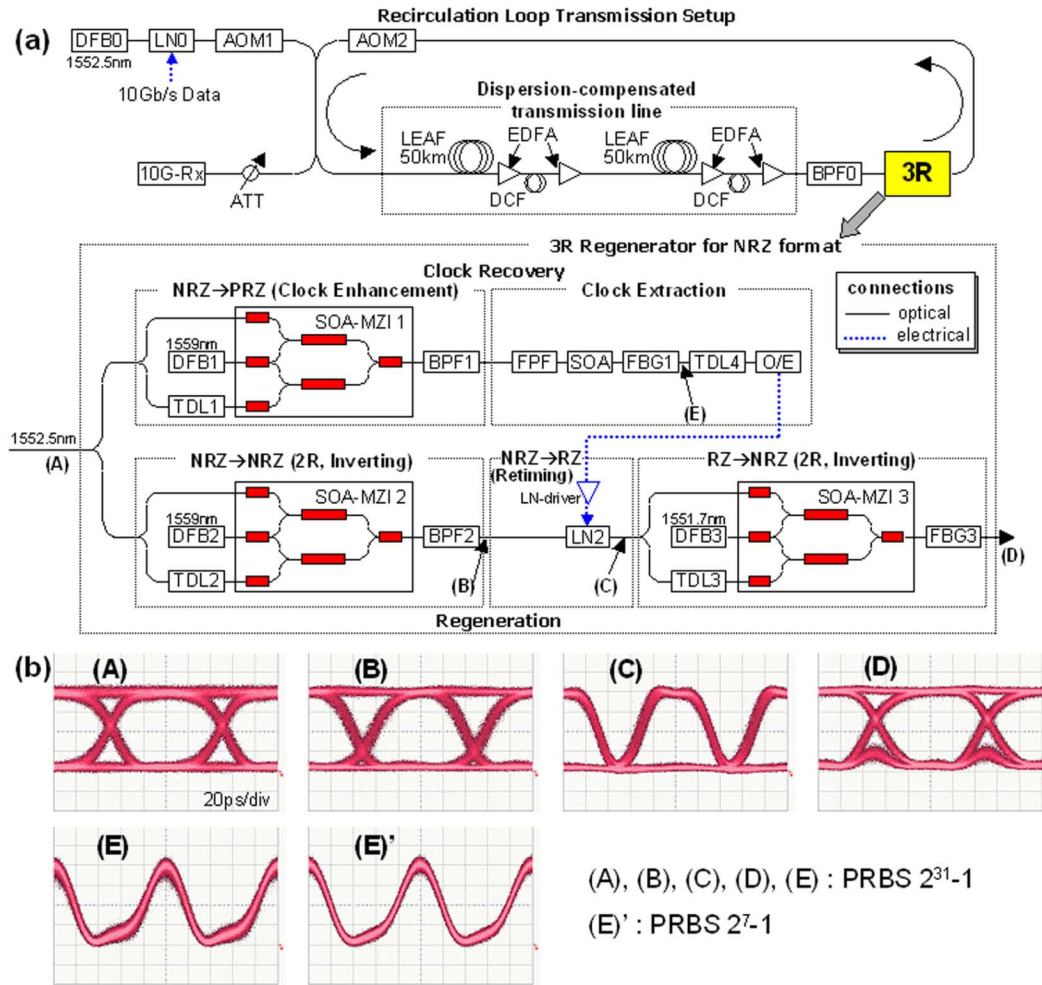


Fig. 16. (a) Experimental setup for optical 3R regeneration of an NRZ signal in a recirculation loop. DFB: distributed feedback laser diode; LN: LiNbO<sub>3</sub>; AOM: acoustooptical modulator; 10G-Rx: 10 Gb/s optical receiver; LEAF: large effective area fiber, DCF: dispersion-compensation fiber; EDFA: erbium-doped fiber amplifier; BPF: bandpass filter; TDL: tunable delay line. (b) Eye diagrams measured at locations (A)–(E) in the setup [10].

the simulation and measurement results show that the jitter accumulation from pattern dependence limits the cascability of the optical 2R regenerator. Full optical 3R regeneration with retiming capability can effectively suppress the jitter accumulation and improve the regenerator cascability [1].

#### IV. EXPERIMENTAL INVESTIGATION OF OPTICAL 3R REGENERATION

The NRZ format is widely used in current wavelength-division multiplexing (WDM) systems for its relatively narrow spectral bandwidth and high tolerance to dispersion effects. However, due to the challenges from optical clock recovery for an NRZ signal and the complexity of all-optical RZ-to-NRZ conversion, only a few previous papers discussed optical 3R regeneration for the NRZ format [24], [25]. Most of these demonstrations employed electrical clock recovery. Recently, we have proposed and demonstrated an optical 3R regenerator employing all-optical clock recovery [10], [26], [27]. In this section, we discuss the effectiveness of optical 3R regeneration to suppress jitter and amplitude noise accumulation and to improve regenerator cascability.

##### A. Optical 3R Regeneration for NRZ Signals

Fig. 16(a) shows the experimental setup and the eye diagram for optical 3R regeneration of a 10 Gb/s NRZ signal [10]. The SOA-MZI1 performs the all-optical NRZ-to-PRZ (pseudo-RZ) conversion to enhance the 10 GHz clock component in the optical signal. The subsequent Fabry–Perot filter (FPF) with a free-spectral range (FSR) of 10 GHz and a finesse of 100 extracts the clock component all-optically [4]. The saturated SOA after the FPF suppresses the pattern-dependent amplitude variation in the recovered clock. The following fiber Bragg grating filter (FBG1, 0.22-nm bandwidth) improves the OSNR of the recovered clock by rejecting the out-of-band ASE noise. In Fig. 16(b), inset (E) shows the optical clock recovered from PRBS 2<sup>31</sup>-1 and the clock in inset (E)' is recovered from PRBS 2<sup>7</sup>-1. The optical-to-electrical converter (O/E) then converts the optical clock into an electrical signal that synchronously modulates the data streaming for retiming [4]. Driven by the recovered clock, the modulator LN2 retimes the reshaped optical NRZ signal from SOA-MZI2 and converts the signal into an RZ format. SOA-MZI3 converts the RZ signal back to the NRZ format. Inset (D) in Fig. 16(b) shows the 3R-regenerated optical NRZ signal.

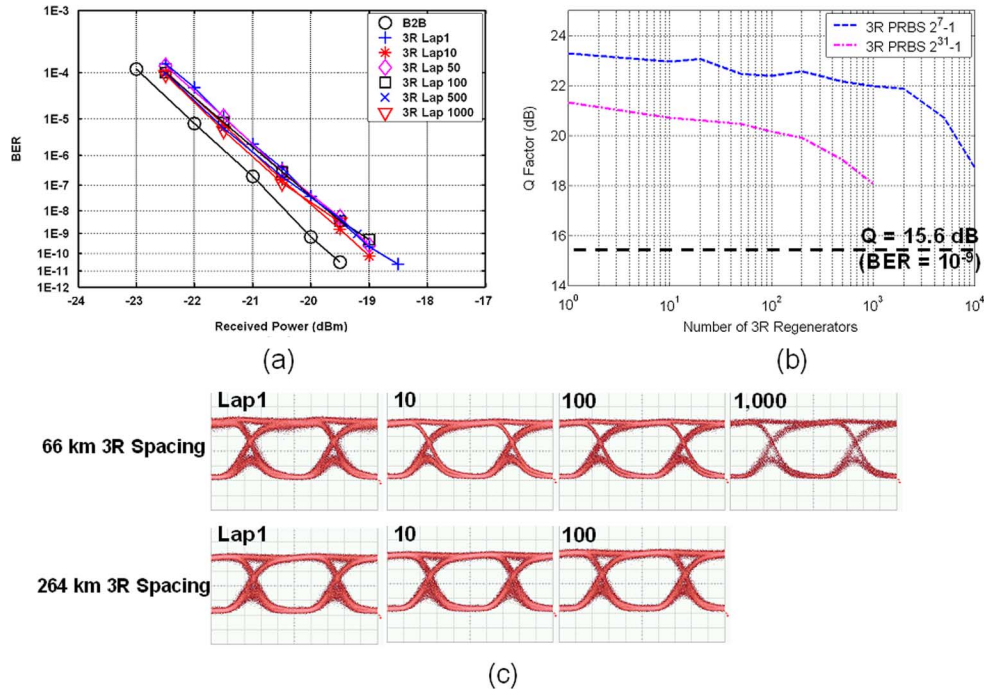


Fig. 17. (a) BER curves for optical 3R regeneration with PRBS  $2^{31}-1$  input, (b) Q-factor evolution for 3R regeneration with PRBS  $2^7-1$  and PRBS  $2^{31}-1$  inputs, and (c) eye diagrams for 3R regeneration with PRBS  $2^7-1$  and PRBS  $2^{31}-1$  inputs.

With a 100 km dispersion-compensated fiber recirculation loop [as shown in Fig. 16(a)], we investigate the cascability improvement of the optical 3R regenerator. Fig. 17(a) shows the BER curves for 3R regeneration with PRBS  $2^{31}-1$  input. Up to lap 100, there is no observable error-floor above BER  $10^{-10}$  in the curves. Fig. 17(b) plots the Q-factor evolution for 3R regeneration with PRBS  $2^7-1$  and PRBS  $2^{31}-1$  inputs. Compared to the results in Fig. 15, the Q-factor results prove that the optical 3R regenerator effectively suppresses the jitter and amplitude noise that limits the cascability of optical 1R and 2R regenerators. The eye diagrams in Fig. 17(c) are also consistent with trend observed in the BER curves and Q-factor evolution. Clean and open NRZ eye diagrams are obtained for PRBS  $2^7-1$  and PRBS  $2^{31}-1$  at lap 10 000 and lap 100, respectively.

### B. Field Trial of Optical 3R Regeneration

While the previous section investigates optical 3R regeneration for an NRZ signal in a well-controlled lab environment, we discuss the assessments of the optical 3R regenerator under relatively realistic field fiber conditions. The field trial experiments substitute the lab fiber in the recirculation loop in Fig. 16 with different lengths of underground fiber links and investigate the optical 3R cascability versus regeneration spacing [26], [27]. One field fiber span consists of 66 km standard single-mode fiber with dispersion compensation, which runs from Burlingame to Palo Alto and loops back. We can obtain various regeneration spacings by including one or multiple spans in the recirculation loop. The experiments adopt 10 Gb/s NRZ signals with PRBS  $2^7-1$  and choose regeneration spacings of 66 and 264 km.

Fig. 18 depicts the field trial experiment results. When the 3R spacing is 66 km, the BER curves in Fig. 18(a) show that there is no observable error floor above BER  $10^{-9}$  up to lap

1000. The Q-factor evolution in Fig. 18(b) exhibits the relation between 3R cascability and 3R spacing. When the spacing is 264 km, the Q factor drops below 15.6 dB (BER =  $10^{-9}$ ) at lap 100. While for 66 km 3R spacing, the Q factor is still above 17 dB at lap 1000. This is because the longer 3R spacing induces larger jitter and amplitude noise accumulation before the optical 3R regenerator and thus makes it more difficult for the regenerator to recover the signal performance. Fig. 18(c) shows the eye diagrams measured for different 3R spacings.

## V. SUMMARY

In optical 2R regeneration systems, the timing jitter becomes the most important limiting factor. We proposed a simulation model to isolate the systematic jitter from the bandwidth limitation and the memory effect. The simulation results show that when the pattern dependence from the memory effect is minimized, the jitter accumulation depends critically on the degree of the regenerative nonlinearity ( $\gamma$  parameter). Increasing the regenerator bandwidth to a larger value than the data rate can relieve the jitter accumulation and slow down the BER increment only when  $\gamma$  is greater than 0.55, since bandwidth increase associates with SNR degradation. When the pattern dependence from the memory effect is considered, the jitter increment versus regeneration hop becomes nonlinear even at a  $\gamma$  value of 0.15. The simulation results indicate that the pattern dependence can severely decrease the cascability of an optical 2R regenerator and make it worse than that of a linear optical amplifier (optical 1R). We verify the simulation model by comparing the results to experimental measurements of an optical 2R regenerator based on SOA-MZI. The comparison shows good matches on the jitter peak-to-peak accumulation, eye diagrams, and Q factors. To overcome the jitter accumulation associated with the optical 2R regeneration, we then experimentally demonstrated an

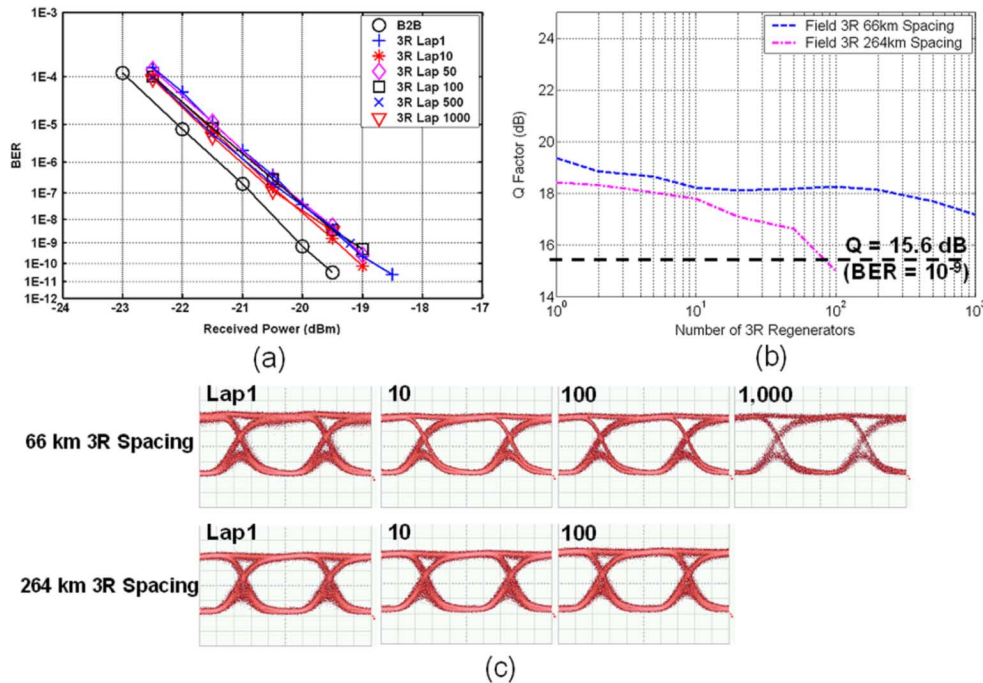


Fig. 18. Field trial experimental results: (a) BER curves for optical 3R regeneration with 66 km spacing, (b) Q-factor evolution for 3R regeneration with 66 and 264 km spacings, and (c) eye diagrams for 3R regeneration with 66 and 264 km spacings.

optical 3R regenerator for optical NRZ signals, which achieved more than 1000-hop cascadability for PRBS  $2^{31} - 1$  inputs with a 100 km recirculation loop using lab fiber. All-optical clock recovery for NRZ signals has been included to provide optical transparency. Field trial experiments then investigated the stability of the optical 3R regenerator in a relatively realistic condition and the tradeoff between the cascadability and regeneration spacing. More than 1000-hop cascadability has been achieved with a 3R spacing of 66 km, and the cascadability decreased to 100-hop at a 3R spacing of 264 km.

#### REFERENCES

- [1] O. Leclerc *et al.*, "Optical regeneration at 40 Gb/s and beyond," *J. Lightw. Technol.*, vol. 21, pp. 2779–2790, Nov. 2003.
- [2] H. N. Poulsen *et al.*, "Transmission enhancement by deployment of interferometric wavelength converters within all-optical cross connects," in *Proc. OFC'97*, Feb. 1997, paper TuO2.
- [3] P. E. Green *et al.*, "WDM protocol-transparent distance extension using R2 remodulation," *J. Sel. Areas Commun.*, vol. 14, pp. 962–967, Jun. 1996.
- [4] Z. Zhu *et al.*, "10 000-hop cascaded in-line all-optical 3R regeneration to achieve 1 250 000-km 10-Gb/s transmission," *IEEE Photon. Technol. Lett.*, vol. 18, pp. 718–720, Mar. 2006.
- [5] P. Ohlen *et al.*, "Noise accumulation and BER estimates in concatenated nonlinear optoelectronic repeaters," *IEEE Photon. Technol. Lett.*, vol. 9, pp. 1011–1013, Jul. 1997.
- [6] J. Mork *et al.*, "Analytical expression for the bit error rate of cascaded all-optical regenerators," *IEEE Photon. Technol. Lett.*, vol. 15, pp. 1479–1481, Oct. 2003.
- [7] D. Marcuse, "Derivation of analytical expression for the bit-error probability in lightwave systems with optical amplifiers," *J. Lightw. Technol.*, vol. 8, pp. 1816–1823, Dec. 1990.
- [8] G. Raybon *et al.*, "40 Gbit/s pseudo-linear transmission over one million kilometers," in *Proc. OFC'02*, Mar. 2002, paper FD10.
- [9] P. Ohlen *et al.*, "Measurements and modeling of pattern-dependent BER and jitter in reshaping optoelectronic repeaters," *Proc. Inst. Elect. Eng. Optoelectron.*, vol. 147, pp. 97–103, Apr. 2000.
- [10] M. Funabashi *et al.*, "Optical clock recovery and 3R regeneration for 10-Gb/s NRZ signal to achieve 10 000-hop cascadability and 1 000 000-km transmission," *IEEE Photon. Technol. Lett.*, vol. 18, pp. 2078–2080, Oct. 2006.
- [11] R. Stephens, "Analyzing jitter at high data rates," *IEEE Commun. Mag.*, vol. 42, pp. 6–10, Feb. 2004.
- [12] Y. Takasaki, *Digital Transmission Design and Jitter Analysis*. Norwood, MA: Artech House, 1991.
- [13] P. R. Trischitta *et al.*, *Jitter in Digital Transmission Systems*. Norwood, MA: Artech House, 1989.
- [14] C. Joergensen *et al.*, "All-optical wavelength conversion at bit rates above 10 Gb/s using semiconductor optical amplifiers," *IEEE J. Sel. Topics Quantum Electron.*, vol. 3, pp. 1168–1180, Oct. 1997.
- [15] C. M. Weinert *et al.*, "Measurement and modeling of timing jitter in optoelectronic repeaters and frequency converters," *IEEE Photon. Technol. Lett.*, vol. 11, pp. 278–280, Feb. 1999.
- [16] P. Ohlen *et al.*, "BER caused by jitter and amplitude noise in limiting optoelectronic repeaters with excess bandwidth," *Proc. Inst. Elect. Eng. Optoelectron.*, vol. 145, pp. 147–150, Jun. 1998.
- [17] B. Mikkelsen *et al.*, "Opto-electronic and all-optical wavelength translators and their cascadability," in *Proc. OFC'99*, Feb. 1999, paper FJ1.
- [18] R. J. S. Pedersen *et al.*, "WDM cross-connect cascade based on all-optical wavelength converters for routing and wavelength slot interchanging using a reduced number of internal wavelengths," in *Proc. OFC'98*, Feb. 1998, paper TuJ2.
- [19] T. Durhuus *et al.*, "All-optical wavelength conversion by semiconductor optical amplifiers," *J. Lightw. Technol.*, vol. 14, pp. 942–954, Jun. 1996.
- [20] R. Ramaswami *et al.*, *Optical Networks a Practical Perspective*, 2nd ed. San Diego, CA: Academic, 2002.
- [21] K. I. Kang *et al.*, "Comparison of sagnac and Mach-Zehnder ultrafast all-optical interferometric switches based on a semiconductor resonant optical nonlinearity," *Appl. Opt.*, vol. 35, pp. 417–426, Jan. 1996.
- [22] P. Guerber *et al.*, "Chirp optimised operation of an optical 3R regenerator," in *Proc. ECOC'00*, Sep. 2000, paper 8.4.4.
- [23] B. Mikkelsen *et al.*, "All-optical noise reduction capability of interferometric wavelength converters," *Electron. Lett.*, vol. 32, pp. 566–567, Mar. 1996.
- [24] D. Chiaroni *et al.*, "New 10 Gbit/s 3R NRZ optical regenerative interface based on semiconductor optical amplifiers for all-optical networks," in *Proc. ECOC'97*, Sept. 1997, vol. 5, pp. 41–44.

- [25] H. S. Chung *et al.*, "40-Gb/s NRZ wavelength conversion with 3R regeneration using an EA modulator and SOA polarization-discriminating delay interferometer," *IEEE Photon. Technol. Lett.*, vol. 18, pp. 337–339, Jan. 2006.
- [26] M. Funabashi *et al.*, "Cascadability of optical 3R regeneration for NRZ format investigated in recirculating loop transmission over field fibers," *IEEE Photon. Technol. Lett.*, vol. 18, pp. 2081–2083, Oct. 2006.
- [27] M. Funabashi *et al.*, "First field demonstration of 1000-hop cascaded all-optical 3R regeneration in 10 Gb/s NRZ transmission," in *Proc. CLEO'06*, May 2006, paper CPDB7.

**Zuqing Zhu** (S'01) received the B.S. degree from the Department of Electronic Engineering and Information Science, University of Science and Technology of China, Hefei, in 2001 and the M.S. degree from the Department of Electrical and Computer Engineering, University of California, Davis, in 2003, where he is currently pursuing the Ph.D. degree.

His research focuses on advanced optical switching and regeneration technologies for the next-generation optical networks.

Mr. Zhu is a student member of the Optical Society of America.

**Masaki Funabashi** received the B.E. and M.E. degrees in electronic engineering from the University of Tokyo, Tokyo, Japan, in 1995 and 1997, respectively.

In 1997, he joined Yokohama R&D Laboratories, The Furukawa Electric Co., Ltd., Yokohama, Japan, where he has engaged in the research and development of long-wavelength semiconductor optical devices, such as distributed feedback lasers, pump lasers, modulators, and waveguide photodiodes. From 2004 to 2006, he was with the University of California, Davis, as a Visiting Researcher, where he studied optical signal regeneration and optical-label switching technologies. His research interests are physics, design, fabrication, and characterization of semiconductor optical devices and their integration and packaging technologies.

**Zhong Pan** (S'01) received the B.S. degree in electrical engineering from Tsinghua University, Beijing, China, in 2000 and the M.S. degree in electrical engineering from the University of California, Davis, in 2002, where he is currently pursuing the Ph.D. degree.

His research focuses on optical-label switching in optical communication networks, especially the control of the tunable laser and its application.

Mr. Pan is a student member of the Optical Society of America.

**Bo Xiang**, photograph and biography not available at the time of publication.

**Loukas Paraschis** was born in Athens, Greece. He received the M.S. and Ph.D. degrees from Stanford University, Stanford, CA, in 1998 and 1999, respectively.

He is Technical Leader in core routing with Cisco Systems, responsible for the next-generation optical technologies, R&D, and network architectures. At Cisco, he has primarily worked on WDM networks, multiservice metro and IP-over-WDM architectures, network availability, and technoeconomical analysis. Previously, he was an R&D Engineer. He has authored or coauthored more than 35 peer-reviewed technical publications, multiple invited, keynote, and tutorial presentations, technical reports, and three patent disclosures. He has been Editor for Optical Networks of the *Journal of Communications and Networks*, a panelist for the National Science Foundation, and a member of conference organizing committees.

Dr. Paraschis was a Co-Guest Editor of the JOURNAL OF LIGHTWAVE TECHNOLOGY (November 2004).

**S. J. Ben Yoo** (S'82–M'84–SM'97) received the B.S. degree (with distinction) in electrical engineering, the M.S. degree in electrical engineering, and the Ph.D. degree in electrical engineering with a minor in physics from Stanford University, Stanford, CA, in 1984, 1986, and 1991, respectively.

He currently is a Professor of electrical engineering at the University of California, Davis (UC Davis) and Director of the UC Davis branch of the Center for Information Technology Research in the Interest of Society. His research at UC Davis includes high-performance all-optical devices, systems, and networking technologies for the next-generation Internet. In particular, he is conducting research on architectures, systems integration, and network experiments related to all-optical label switching routers and optical code-division multiple-access technologies. Prior to joining UC Davis in 1999, he was a Senior Research Scientist with Bell Communications Research (Bellcore), leading technical efforts in optical networking research and systems integration. His research activities at Bellcore included optical label switching for the next-generation Internet, power transients in reconfigurable optical networks, wavelength interchanging cross-connects, wavelength converters, vertical-cavity lasers, and high-speed modulators. He also participated in the advanced technology demonstration network/multiwavelength optical networking (ATD/MONET) systems integration, the OC-192 synchronous optical network (SONET) ring studies, and a number of standardization activities that led to documentations of generic requirements GR-2918-CORE (1999), GR-2918-ILR (1999), GR-1377-CORE (1995), and GR-1377-ILR (1995) on dense wavelength-division multiplexing and OC-192 systems. Prior to joining Bellcore in 1991, he conducted research at Stanford University on nonlinear optical processes in quantum wells, a four-wave-mixing study of relaxation mechanisms in dye molecules, and ultrafast diffusion-driven photodetectors. During this period, he also conducted research on lifetime measurements of intersubband transitions and on nonlinear optical storage mechanisms with Bell Laboratories and IBM Research Laboratories, respectively.

Prof. Yoo is a Senior Member of the IEEE Lasers and Electro-Optics Society (LEOS) and a member of the Optical Society of America (OSA) and Tau Beta Pi. He received the DARPA Award for Sustained Excellence in 1997, the Bellcore CEO Award in 1998, and the Mid-Career Research Faculty Award (UC Davis) in 2004. He was Cochair of the Technical Program Committee for APOC 2004 and APOC 2003, and Technical Program Committee Member for CLEO'2005, CLEO'2004, CLEO'2003, LEOS'2000, LEOS'1999, LEOS'1998, OECC/COIN'2004, COIN'2003, COIN'2002, NLGA'2000, and OAA'2005. He is an Associate Editor for IEEE PHOTONICS TECHNOLOGY LETTERS.